ChemComm

Accepted Manuscript

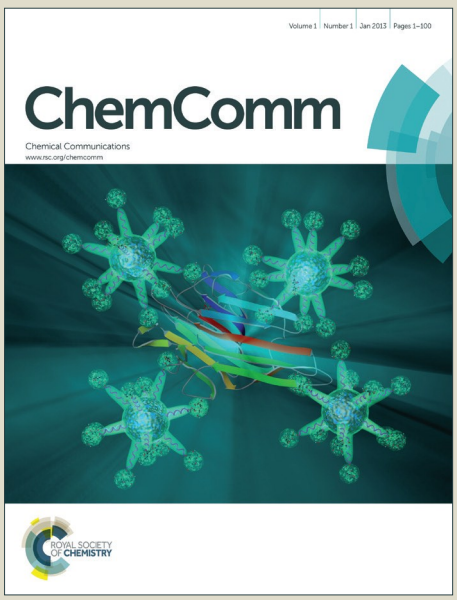

ROYAL SOCIETY OF CHEMISTRY

www.rsc.org/chemcomm

Journal Name

COMMUNICATION

Hydrogenated $CeO_{2-x}S_x$ mesoporous hollow spheres for enhanced solar driven water oxidation

Received 00th January 20xx,
Accepted 00th January 20xx

DOI: 10.1039/x0xx00000x

www.rsc.org/

Yuting Xiao, Yajie Chen, Ying Xie, Guohui Tian*, Shien Guo, Taoran Han and Honggang Fu*

A facile route for the fabrication of hydrogenated sulfur-doped CeO_2 (H-$CeO_{2-x}S_x$) mesoporous hollow spheres. It exhibited excellent photocatalytic activity due to the synergistic effect of higher sulfur doping level and hydrogen post-treatment.

Photocatalytic water splitting is thought as one economically viable approach to the direct conversion of solar energy into renewable and storable hydrogen and oxygen.[1,2] Compared to the reduction half-reaction, the oxygen evolution reaction is the most difficult half reaction in water splitting, involving the transfer of four electrons and the formation of oxygen-oxygen bonds.[3] So an efficient oxygen evolution catalyst is essential to enhance the reaction rate. CeO_2 is an attractive material for photocatalytic water oxidation because of its suitable valence band level for this reaction.[4] However, the wide bandgap (≈3.0 eV) similar to TiO_2 renders CeO_2 only responsive to UV light, which accounts for less than 5% of the solar energy.[5] In view of solar utilization, it is of critical importance to improve its visible-light photocatalytic capability.

Previous studies showed the introduction of doping agents into semiconductor could produce oxygen vacancy and reduce the semiconductor electronic band gap or create localized electronic states in the band gap that could improve the direct absorption of visible light, and also serve as the active sites to improve the carrier separation efficiency.[6] By virtue of the redox potentials of cerium (III) and cerium (IV), CeO_2 can easily form nonstoichiometric compositions (CeO_{2-x}) by cation doping, leaving oxygen vacancies in the lattice.[7,8] Recent studies also confirmed that the incorporation of Sulfur element increased visible-light photocatalytic activity compared with pristine semiconductor.[9] But the enhancement of photocatalytic performance is not apparent due to the low Sulfur content.

Hydrogenation of semiconductors was proved to be another effective approach to extend optical absorption range and increase the photocatalytic performance by the introduction of oxygen vacancies to the surface of semiconductors.[10,11] The produced oxygen vacancies were demonstrated to be electron donors in semiconductors and considered to contribute to the enhanced donor density and Fermi level shift, accelerating charge separation at the semiconductor/solution interface.[12,13] Besides, surface and structural properties of catalysts, e.g. surface area and morphology, greatly influenced water oxidation reactions as well.[14] For instance, CeO_2 hollow spheres have been reported to show enhanced ultraviolet light photocatalytic water splitting ability in comparison to bulk catalysts owing to the advantages of low density, increased surface area and enhanced light-harvesting efficiency.[15,16] Despite the significant contributions have been made in this area , it is still desirable to improve solar light or visible photocatalytic activity of CeO_2-based semiconductors.

Inspired by the pioneer work, herein, we report a facile route for the fabrication of hydrogenated sulfur-doped CeO_2 (H-$CeO_{2-x}S_x$) mesoporous hollow spheres via a two-step procedure, as illustrated

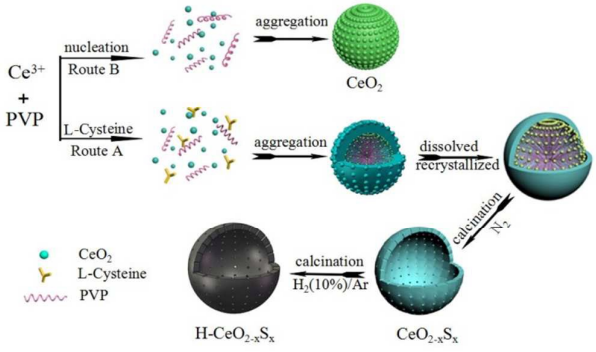

Scheme 1 Schematic illustration of the preparation of hydrogenated sulfur-doped CeO_2 (H-$CeO_{2-x}S_x$) mesoporous hollow spheres: (A) Hydrothermal synthesis of sulfur-doped CeO_2 ($CeO_{2-x}S_x$) mesoporous hollow spheres with L-Cysteine as starting material for preparation of corresponding hydrogenated product (H-$CeO_{2-x}S_x$). (B) Hydrothermal synthesis without L-Cysteine leads to CeO_2 solid spheres.

Key Laboratory of Functional Inorganic Material Chemistry, Ministry of Education of the People's Republic of China, Heilongjiang University, Harbin 150080 P. R. China. E-mail: tiangh@hlju.edu.cn, fuhg@vip.sina.com

Electronic Supplementary Information (ESI) available: [details of any supplementary information available should be included here]. See DOI: 10.1039/x0xx00000x

in Route A in the Scheme 1. Sulfur doped CeO_2 ($CeO_{2-x}S_x$) mesoporous hollow spheres were first prepared via a simple hydrothermal and calcination process in N_2 atmosphere. The subsequent hydrogen post-treatment produced hydrogenated $CeO_{2-x}S_x$ mesoporous hollow spheres. The introduction of high content sulfur and the creation of surface oxygen vacancies can promote the light harvesting performance and carrier separation efficiency of CeO_2 through accumulative and synergistic effects, thereby resulting in significantly improved water oxidation performance and excellent stability under solar irradiation.

The crystallographic structures of the as prepared samples were examined by X-ray powder diffraction (XRD). As shown in Fig. S1 (ESI†), the major reflections for the samples appeared at 2ϑ values of 28.51, 33.02, 47.36, 56.28, and 58.97 matched to the cubic fluorite structure CeO_2 (PDF# 00-043-1002).[17] In comparison with pure CeO_2, no evident difference can be observed except for the gradual decrease in peak intensity and peak broadening for the $CeO_{2-x}S_x$, and H-$CeO_{2-x}S_x$. It reveals the crystallinity of $CeO_{2-x}S_x$ and H-$CeO_{2-x}S_x$ gradually reduces while the basic structure of CeO_2 does not change after sulfur doping and hydrogen post-treatment. Structural properties of the samples were further examined by confocal micro-Raman spectroscopy and XPS analysis.

The hollow morphology of the as-synthesized $CeO_{2-x}S_x$ and H-$CeO_{2-x}S_x$ can be proved by scanning electron microscope (SEM) and transmission electron microscopy (TEM) as shown in Fig. 1A-E. The diameter of hollow spheres is around 500 nm. The inner hollow structure can be observed more clearly from the broken spheres (Fig. 1C) as labeled and TEM image (Fig. 1E). For $CeO_{2-x}S_x$ sample, mesopores consisted by crystalline nanoparticles can also be found in HRTEM image (Fig. 1G). A well-defined crystalline lattice can be identified with a d-spacing of 0.31 nm and 0.27 nm corresponds well with the characteristic (111) and (200) planes of CeO_2, respectively.[18] As shown in Fig. 1D, after hydrogen post-treatment, the obtained H-$CeO_{2-x}S_x$ sample still kept the pristine hollow structure morphology without collapse. A thin disordered surface layer can also be observed (indicated by white arrows in Fig. 1F), further demonstrating the successful hydrogenation. A well-defined crystalline lattice can be identified with a d-spacing of 0.31 nm corresponding to the (111) plane of CeO_2, in good agreement with the XRD result (Fig. S1 ESI†).

It should be emphasized here that the use of L-Cysteine as the sulfur source and polyvinylpyrrolidone (PVP) as the shape modifier is critical for the formation of sulfur doped mesoprous hollow spheres. As is shown in Route B in Scheme 1, when the synthesis is carried out in the absence of L-Cysteine, only surface-roughed CeO_2 solid spheres with the diameter around 200 nm were formed (Fig. S2 ESI†). In our experiment, L-Cysteine is abundant, and acts as both sulfur source and micelle to coordinate with Ce(III) ions via its functional groups, such as –SH, –NH_2, –COOH. During the initial stage of the reaction, the sulfur doped cerium oxide nanoparticles (Fig. S3A ESI†) are produced via the aqueous solution (Route A in Scheme 1). With the extension of reaction time, the sulfur-doped CeO_2 nanoparticles tend to assemble into hollow spherical agglomerates (Fig. S3B ESI†) driven from cross-linked micelle templates and by reducing the surface energy of nanoparticles.[19] Meanwhile hydrogen sulfide gas produced from reaction process maybe plays a positive role in enlarging hollow structure (Fig. S3C ESI†). After further dissolution and recrystallization, hollow spheres with smooth surface were formed (Fig. S3D ESI†). The following calcination in nitrogen atmosphere produced mesoporous structure via the removal of organic materials. Finally the H-$CeO_{2-x}S_x$ mesoporous hollow spheres were obtained via the hydrogen post-treatment. In this reaction system, the synergistic effect of L-Cysteine and PVP plays a pivotal role, without the presence of PVP, the morphology of the product was irregular (Fig. S4 ESI†). In addition, this reaction requires relatively high activation energy. When the reaction temperature is blow 160 ^{o}C , no solid product can be obtained because of the insufficient energy.

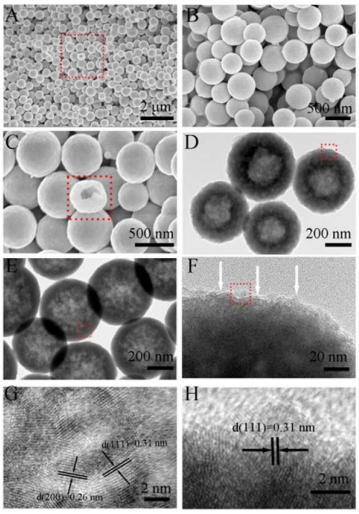

Fig. 1 SEM images with different magnification (A, C), TEM (E) and HRTEM (G) images of the $CeO_{2-x}S_x$; SEM image (B), TEM (D) and HRTEM (F, H) images of the H-$CeO_{2x}S_x$.

The compositions and chemical states of H-$CeO_{2-x}S_x$ compared to CeO_2 were first studied by X-ray photoelectron spectroscopy (XPS). The existence of sulfur signals in the XPS spectra of $CeO_{2-x}S_x$ and H-$CeO_{2-x}S_x$ can be clearly seen in Fig. S5 (ESI†). Meanwhile, three broadened peaks of S 2p at around 163.6, 168.1 and 170.3 eV (Fig. 2A) were assigned to S_n^{2-}, SO_3^{2-} and SO_4^{2-}, ascribing to substitutional and interstitial S dopants, respectively.[20] The results suggested that S species had been successfully incorporated into CeO_2, even after hydrogen post-treatment. For XPS spectrum of O 1s (Fig. 2B), three peaks are observed. The first peak at around 529.1 eV can be attributed to lattice oxygen (O^{2-}) in the CeO_2 lattice, the second peak at around 531.4 eV corresponds to adsorbed oxygen species by hydroxyl species, while the rest peak corresponds to adsorbed water on the surface and chemisorbed oxygen.[21] The Ce 3d XPS spectra of the samples can be assigned to $3d_{3/2}$ spin-orbit states (labeled U) and $3d_{5/2}$ states (labeled V).[22] The spectra of 885.9 eV (V^{I}) and 904.5 eV (U^{I}) assigned to Ce^{3+} are observed in all samples except pure CeO_2, which is consistent with the previous report of Ce^{3+}, implying that Ce exists in mixed valence states (Ce^{4+} and Ce^{3+}) in $CeO_{2-x}S_x$ and H-$CeO_{2-x}S_x$.[23] This indicates the possibility of S_n^{2-} into CeO_2 lattice, together with hydrogen post-treatment, caused charge imbalance and lattice distortion of CeO_2, so oxygen vacancies are formed.

Structural properties of the samples were also examined by Raman spectroscopy. As shown in Fig. 2D, the peak at 459 cm^{-1}, as

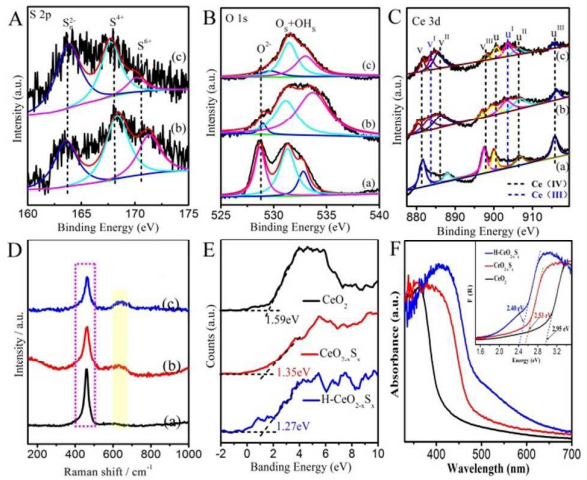

Fig. 2 High-resolution XPS scans of (A) S2p, (B) O1s, (C) Ce3d and (D) Laser Raman spectra of (a) CeO_2, (b) $CeO_{2-x}S_x$, and (c) H-$CeO_{2-x}S_x$. (E) Valence band XPS spectra. (F) UV–vis diffuse reflectance spectra and corresponding band gap energies (inset) of CeO_2, $CeO_{2-x}S_x$, and H-$CeO_{2-x}S_x$.

observed in the pure CeO_2, is the characteristic of the stoichiometric CeO_2 and mainly arises due to the *F*2g skeletal vibration of cubic fluorite structure.[24] While in the enlarged view of Raman spectra in the region of 420 - 500 cm^{-1} (Fig. S6 ESI†), for $CeO_{2-x}S_x$ and H-$CeO_{2-x}S_x$, the Raman peak at 459 cm^{-1} shifts to 461 cm^{-1} and 465 cm^{-1}, respectively. These shifts can be attributed to the increase defects in the crystalline within the nanocomposites as a result of the distortion caused by the embedded sulfur element. Meanwhile, an additional band at approximately 620 cm^{-1} can also be found in Raman spectra of both $CeO_{2-x}S_x$ and H-$CeO_{2-x}S_x$. This can be attributed to the increase in the localized defects associated with oxygen vacancies caused by the embedded sulphur and hydrogen post-treatment.

The concentration of oxygen vacancies was determined by a numerical double integration of the EPR spectra recorded at 300 K. As shown in Fig. S7 (ESI†), $CeO_{2-x}S_x$ and H-$CeO_{2-x}S_x$ exhibit an EPR signal at g = 2.003 after sulfur doping and hydrogen post-treatment, which could be identified as the electrons trapped by oxygen vacancies.[6,13] As expected, the H-$CeO_{2-x}S_x$ sample shows higher EPR signal intensity than $CeO_{2-x}S_x$, confirming that the content of oxygen vacancies increases after hydrogen post-treatment, which agrees with the XPS result in Fig. 2C.

As the thin disordered surface layer structure was formed, the H-$CeO_{2-x}S_x$ sample was colorized deep brown (Fig. S8 ESI†). Compared with pristine CeO_2 (pale yellow powders) and the $CeO_{2-x}S_x$ (brown powders), H-$CeO_{2-x}S_x$ sample significantly enhanced the absorption of visible light as shown in Fig. 2F. The band gap energies of CeO_2, $CeO_{2-x}S_x$, and H-$CeO_{2-x}S_x$ were determined to be 2.95, 2.53, and 2.40 eV, respectively. The gradual decrease of the band gap energies is supported by the results of density functional theory calculations (Fig. S9 ESI†). Together with the valence band XPS analysis (Fig. 2E), the energy band diagram (Fig. S10 ESI†) of CeO_2, $CeO_{2-x}S_x$ and H-$CeO_{2-x}S_x$ were built. It is suggested that a blue shift of the maximum energy of CeO_2 is induced by sulfur doping and hydrogen post-treatment, the valence band tail states extended above the valence band maximum for 0.32 eV, and the conduction band tail states probably extended below the conduction band minimum for 0.23 eV. Evidently, the calculated density of states (DOS) in Figure S9 (ESI†) also proved that the H-$CeO_{2-x}S_x$ sample had an obviously increased DOS at the conduction band edge compared with the CeO_2 and $CeO_{2-x}S_x$ counterparts, which indicates that more carriers can be effectively transferred to the conduction band minimum of the H-$CeO_{2-x}S_x$.[25] The existence of midgap states causes the enhancement of visible light absorption of H-$CeO_{2-x}S_x$, which is probably the reason for the relatively good photocatalytic performance.[26]

Fig. S11 (ESI†) shows that the N_2 adsorption–desorption isotherms of H-$CeO_{2-x}S_x$ and $CeO_{2-x}S_x$ are ascribed to type IV isotherm according to the IUPAC classification.[27] The isotherms of H-$CeO_{2-x}S_x$ and $CeO_{2-x}S_x$ mesoporous hollow spheres show typical H3 hysteresis loop characteristic of mesoporous solids. The BET surface areas of the H-$CeO_{2-x}S_x$ and $CeO_{2-x}S_x$ are 124 $m^2 g^{-1}$ and 106 $m^2 g^{-1}$, respectively, which are almost more than five times as large as that of pure CeO_2 , suggesting that H-$CeO_{2-x}S_x$ and $CeO_{2-x}S_x$ could provide more active sites for catalytic reactions. The H-$CeO_{2-x}S_x$ and $CeO_{2-x}S_x$ have narrow BJH adsorption pore size distribution with a mean value of 4.5 nm, implying that the materials have regular pore structures in the mesoporous region.

The photocatalytic performance of the as-prepared samples was evaluated in a test of the photocatalytic water oxidation reaction. As shown in Fig. 3A, it is evident that the oxygen evolution rates of the S-doped CeO_2 samples ($CeO_{2-x}S_x$) are much higher than that of pure CeO_2 because of sulfur doping. Moreover, sulfur doping content has influence on the photocatalytic activity, with the increase of sulfur content, the oxygen evolution rates of the $CeO_{2-x}S_x$ samples first increased and then decreased, and the $CeO_{2-x}S_x$-2.5 (the molar ratio of Ce to S at 1:2.5) exhibited the best oxygen evolution rate of 37 μmol h^{-1} under AM1.5 irradiation. Selecting the optimum S-doped CeO_2 ($CeO_{2-x}S_x$-2.5) as hydrogenated objective, and the hydrogenated product was named as H-$CeO_{2-x}S_x$. The average O_2 generation rate (91 μmolh^{-1}) of H-$CeO_{2-x}S_x$ under AM1.5 irradiation is 7 and 2 times higher than that of the pristine CeO_2 (12 μmolh^{-1}) and $CeO_{2-x}S_x$ (37 μmolh^{-1}), respectively. This unambiguously indicates that the H-$CeO_{2-x}S_x$ can act as an efficient photocatalyst for oxygen evolution from water oxidation. Moreover, the visible-light oxygen generation of both H-$CeO_{2-x}S_x$ and $CeO_{2-x}S_x$ are more efficient than CeO_2, the oxygen generation of H-$CeO_{2-x}S_x$ (22 μmolh^{-1}) is much higher than that of $CeO_{2-x}S_x$ (13 μmolh^{-1}). Meanwhile, no noticeable decrease in O_2 production rate for the H-$CeO_{2-x}S_x$ throughout the testing cycles under AM1.5 irradiation was observed, indicating its high stability (Figure 3D). As a control sample, the prepared hydrogenated CeO_2 (H-CeO_2) solid spheres exhibited inferior oxygen evolution activity (Fig. S12 ESI†).

Meanwhile, the normalized oxygen evolution amount of the H-$CeO_{2-x}S_x$ is also higher than that of the others, it indicated that the larger amount of O_2 produced by the H-$CeO_{2-x}S_x$ could be attributed to the synergistic effect of its stronger visible-light absorption, larger surface area as well as higher carrier separation efficiency due to the presence of proper content of oxygen vacancies. As described earlier, larger visible-light absorption caused by narrowed band gap can excite more photogenerated charges. Porous hollow structure with higher surface area can provide enhanced number of

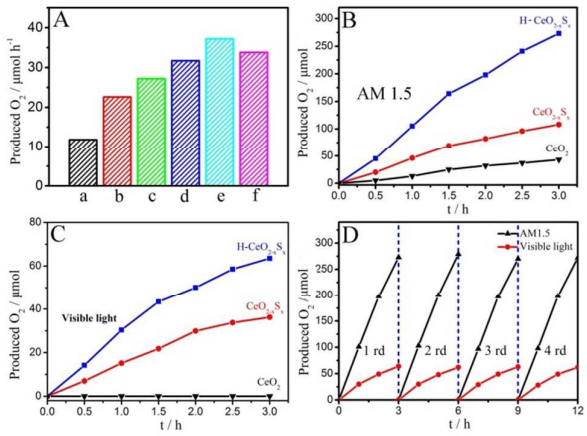

Fig. 3 (A) O_2 evolution reaction of $CeO_{2-x}S_x$ with different contents of S, a: CeO_2, b: $CeO_{2-x}S_x$-1, c: $CeO_{2-x}S_x$-1.5, d: $CeO_{2-x}S_x$-2, e: $CeO_{2-x}S_x$-2.5 and f: $CeO_{2-x}S_x$-3 under AM1.5 irradiation; time course of produced O_2 for the different samples under (B) AM1.5 irradiation, (C) visible light irradiation, (D) repeated O_2 evolution test of H-$CeO_{2-x}S_x$ under AM1.5 and visible light irradiation (λ≥400 nm).

reaction sites compared with the solid spheres (Fig. S13 ESI†). Moreover, the presence of proper content of oxygen vacancies endows the H-$CeO_{2-x}S_x$ mesoporous hollow spheres with increased density of states (DOS) at valence band maximum and conduction band minimum (Fig. S9 ESI†), which can assure a higher carrier concentration and thus increase the electric field in the space charge regions for acquiring enhanced carrier separation.[28,13] Electrochemical tests also proved the efficient charge separation. As shown in Fig. S14A (ESI†) , the photocurrent density obtained on H-$CeO_{2-x}S_x$ is enhanced as compared to that of $CeO_{2-x}S_x$ and CeO_2 under visible light irradiation, which suggests the longer life span achieved on the H-$CeO_{2-x}S_x$ sample. The electrochemical impedance spectroscopy (EIS) Nyquist plots shown in Fig. S14B (ESI†) reveal the H-$CeO_{2-x}S_x$ electrode exhibits decreased arc at high frequency under visible light irradiation compared to $CeO_{2-x}S_x$ and CeO_2 electrodes, which indicates its good conductivity and more efficient charge separation. Besides, the enhanced photocatalytic performance of the H-$CeO_{2-x}S_x$ mesoporous hollow spheres was further confirmed by the degradation of nitrobenzene under visible light irradiation (Fig. S15 ESI†).

In summary, we demonstrated the synthesis of hydrogenated sulfur-doped CeO_2 (H-$CeO_{2-x}S_x$) mesoporous hollow spheres as O_2-evolving photocatalyst by a facile hydrothermal route and hydrogen post-treatment. Higher sulfur doping level can be maintained even after hydrogen post-treatment. Moreover, experiments and first principle calculations disclose that the O-vacancies lead the H-$CeO_{2-x}S_x$ to possess a new donor level near conduction band minimum and a higher density of states at valence band maximum, which endow the H-$CeO_{2-x}S_x$ with a narrowed band gap and higher carrier concentration, so contributing to the visible light harvesting and the carrier separation efficiency. Together with the superior hollow mesoporous sphere structure, the H-$CeO_{2-x}S_x$ sample exhibited much greater photocatalytic activity than pure CeO_2 and $CeO_{2-x}S_x$ not only under AM1.5 irradiation but also under visible light irradiation. These findings could shed light on the deep understanding of photoreactivity of semiconductors and the fine manipulation of their photoreactivity as well as the development of new photocatalysts.

This research was supported by the National Natural Science Foundation of China (51272070, 21371053, 21376065), Natural Science Foundation of Heilongjiang Province of China (E201455).

Notes and references

1 N. Armaroli and V. Balzani, *Angew. Chem. Int. Ed.,* 2007, **46**, 52.
2 K. Maeda, K.Teramura, D. L. Lu, T. Takata, N. Saito, Y. Inoue and K. Domen, *Nature,* 2006, **440**, 295.
3 Q. X. Mi, A. Zhanaidarova, B. S. Brunschwig, H. B. Gray and N. S. Lewis, *Energy Environ. Sci.*, 2012, **5**, 5694–5700.
4 G. R. Bamwenda, T. Uesigi, Y. Abe, K. Sayama and H. Arakawa, *Appl. Catal. A,* 2001, **205**, 117.
5 T. Hisatomi, T. Minegishi and K. Domen, Bull. *Chem. Soc. Jpn.,* 2012, **85**, 647.
6 T. Q. Lin, C. Y. Yang, Z. Wang, H. Yin, X. L. Lu, F. Q. Huang, J. H. Lin, X. M. Xie and M. H. Jiang, *Energy Environ. Sci.,* 2014, **7**, 967.
7 J. Cafun, K. O. Kvashnina, E. Casals, V. F. Puntes and P. Glatzel, *ACS Nano.,* 2013, **7**, 10726.
8 A. D. Liyanage, S. D. Perera, K. Tan, Y. Chabal and K. J. Balkus, *ACS Catal.,* 2014, **4**, 577.
9 G. Liu, P. Niu, C. H. Sun, S. C. Smith, Z. G. Chen, G. Q. Lu and H. M. Cheng, *J. Am. Chem. Soc.,* 2010, **132**, 11642.
10 Y. H. Hu, *Angew. Chem. Int. Ed.,* 2012, **51**, 12410.
11 W. Zhou, W. Li, J. Q. Wang, Y, Qu, Y. Yang, Y. Xie, K. F. Zhang, L. Wang, H. G. Fu and D. Y. Zhao, *J. Am. Chem. Soc.*, 2014, **136**, 9280.
12 F. C. Lei, Y. F. Sun, K. T. Liu, S. Gao, L. Liang, B. C. Pan and Y. Xie, *J. Am. Chem. Soc.,* 2014, **136**, 6826.
13 A. Naldoni, M. Allieta, S. Santangelo, M. Marelli, F. Fabbri, S. Cappelli, C. L. Bianchi, R. Psaro and V. D. Santo, *J. Am. Chem. Soc.,* 2012, **134**, 7600.
14 G. H. Tian, Y. J. Chen, W. Zhou, K. Pan, Y. Z. Dong, C. G. Tian and H. G. Fu, *J. Mater. Chem.,* 2011, **21**, 887.
15 J. Qi, K. Zhao, G. D. Li, Y. Gao, H. J. Zhao, R. B. Yu and Z. Y. Tang, *Nanoscale,* 2014, **6**, 4072.
16 Y. G. Wang, F. Wang, Y. T. Chen, D. F. Zhang, B. Li, S. F. Kang, Xi Li and L. F. Cui, *Appl. Catal. B,* 2014, **147**, 602.
17 L. Ma, D. S. Wang, J. H. Li, B. Y. Bai, L. X. Fu and Y. D. Li, *Appl. Catal. B,* 2014, **148**, 36.
18 Z. J. Yang, D. Q. Han, D. L. Ma, H. Liang, L. Liu and Y. Z. Yang, *Cryst. Growth Des.,* 2010, ***10***, 291.
19 Y. S. Li and J. L. Shi, *Adv. Mater.,* 2014, **26**, 3176.
20 Z. J. Tan, P. R. Liu, H. M. Zhang, Y. Wang, M. A. Mamun, H. G. Yang, D. Wang, Z. Y Tang and H. J. Zhao, *Chem. Commun.,* 2015, **51**, 5695.
21 Y. Hong, C. G.Tian, B. J. Jiang, A. P. Wu, Q. Zhang, G. H. Tian and H. G. Fu, *J. Mater. Chem. A,* 2013, **1**, 5700.
22 M. Batista, M. N. Cerezo, A. Kubacka, D. Tudela and M. F. García, *ACS Catal.,* 2014, **4**, 63.
23 Y. Yang, C. G. Tian, L. Sun, R. J. Lü, W. Zhou, K. Y. Shi, K. Kan, J. C. Wang and H. G. Fu, *J. Mater. Chem. A,* 2013, **1**, 12742.
24 G. N. Li, L. Li, D. Jiang, Y. S. Li and J. L. Shi, *Nanoscale,* 2015, **7**, 5691.
25 Y. W. Liu, H. Cheng, M. J. Lyu, S. J. Fan, Q. H. Liu, W. S. Zhang, Y. D. Zhi, C. M. Wang, C. Xiao, S. Q. Wei, B. J. Ye and Y. Xie, *J. Am. Chem. Soc.,* 2014, **136**, 15670.
26 R. Shi, T. G. Xu, L. H. Yan, Y. F. Zhu and J. Zhou, *Catal. Sci. Technol.,* 2013, **3**, 1757.
27 P. F. Ji, J. L. Zhang, F. Chen and M. Anpo, *J. Phys. Chem. C,* 2008, **112**, 17809.
28 P. Hartmann, T. Brezesinski, J. Sann, A. Lotnyk, J. P. Eufinger, L. Kienle and J. Janek, *ACS Nano,* 2013, **7**, 2999.